Journal of Drug Delivery Science and Technology 94 (2024) 105411

Contents lists available at ScienceDirect

Journal of Drug Delivery Science and Technology

journal homepage: www.elsevier.com/locate/jddst

The effect of 3D printed microfluidic array designs on the preparation of liposome nanoparticles

Kanza Rahali [a], Atabak Ghanizadeh Tabriz [b], Dennis Douroumis [a,b,*]

[a] Centre for Research Innovation, University of Greenwich, Medway Campus, Kent, ME4 4TB, UK
[b] Delta Pharmaceutics Ltd., Chatham, Kent, ME4 4TB, UK

ARTICLE INFO

Keywords:
3D printing
Digital light processing
Microfluidics
Herringbone
Liposomes
Nanoparticle

ABSTRACT

In this study Digital Light Processing (DLP) was used to manufacture microfluidic arrays with complex geometries for the fabrication of stable liposome nanoparticles. For the purposes of the study three different microfluidic array designs were 3D printed featuring herringbone structures.

The effect of the herringbone numbers and the length of the microfluidic channels on the formation of liposomes was investigated by varying the Total Flow Rate (TFR) and the Flow Rate Ratio (FRR). Laser diffraction analysis showed the production of liposomes with reproducible particle sizes and narrow polydispersity index. The obtained particle size was affected by the TFR (3, 5 and 10 ml/min) and FRR (8:2 and 6:4) varying from 40 to 90 nm. However, the number of herringbone structures in the printed microfluidic arrays demonstrated no significant variations on the liposome particle sizes. Stability studies of the formed nanoparticles showed no changes for the 8:2 FRR and small increase of 8–10 nm for the 6:4 respectively. Overall, the study demonstrated the 3D printing capabilities for the printing of complex microfluidic arrays and the successful engineering of liposomes.

1. Introduction

In the last three decades more than fifty nanoparticulate drug product have been approved by the Food and Drug Administration (FDA) regulatory authority or are under clinical evaluation [1–3]. This includes a wide range of drug delivery systems (DDS) such as lipid and polymer nanoparticles [4,5] that find applications in cancer treatment and regenerative medicine for the delivery of anti-cancer agents, genetic material, vaccines, or even biomimetic materials [6–9]. The latter have found applications in cancer therapy as they facilitate coating of NPs allowing them to interact with cancer cell line, also called 'tumour--homing effect, all the way to binding different proteins on the Biomimetic NPs surface for better targeting [10,11]. The efficient delivery of such DDS depends on the particle size, zeta potential, rigidity, composition, and surface modification. Those properties affect the circulation time, biodistribution and delivery at the targeted site [12–14]. During the COVID-19 pandemic, the manufacturing and scale up of lipid-based vaccines to meet the patient demand became a major concern and raised interest for the usage of emerging manufacturing techniques.

LNPs preparation methods are classified to top-down and bottom-up techniques which can be effectively used to control the obtained particle size which in turn influences the *in vivo* biodistribution, uptake, and clearance [15]. Many of these approaches present drawbacks such as batch to batch variability, difficulties to scale up and large capital investment. Hence there is a need for such cost-effective technologies with small footprint, capability of processing a wide range of materials, control over the nanoparticle properties and scalable manufacturing. An emerging bottom-up technology that has been successfully used for particle size engineering of nanoparticles are microfluidics [16–18]. Some of the main features are the handling of small volumes of fluids and superior mixing in narrow channels of tens to hundreds of micrometers [19]. The fluids are pumped into the channels and mixed using different techniques. The flow inside the narrow channels can be either turbulent or laminar.

The mixing process inside the channels called micromixing, can be either active by applying an external pressure [20,21] or passive by changing the fluids' hydrodynamic using different shapes of channels such as Staggered Herringbone Mixer (SHM), originally developed by Stroock et al. [22]. It is formed by repeated patterns of grooves, each one of them is composed of two different length channels connected to each other, one relatively longer and the other relatively shorter, and those

* Corresponding author. Centre for Research Innovation (CRI), University of Greenwich, Chatham Maritime Kent, ME4 4TB, UK.
E-mail address: D.Douroumis@gre.ac.uk (D. Douroumis).

https://doi.org/10.1016/j.jddst.2024.105411
Received 22 September 2023; Received in revised form 9 January 2024; Accepted 23 January 2024
Available online 7 February 2024

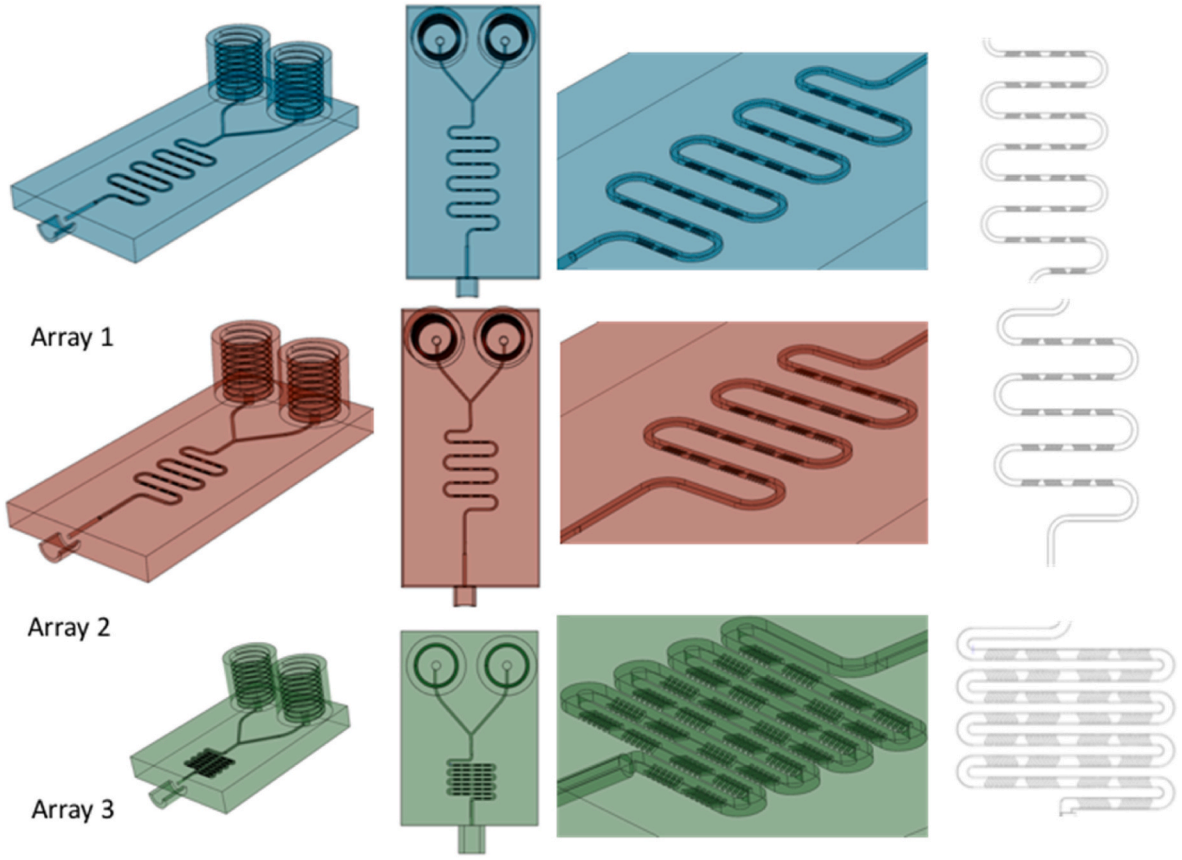

Fig. 1. Schematic illustration of microfluidic Arrays (1–3) with herringbone micromixture structures designed using SolidWorks.

two grooves meet with a certain angle, usually 45° [20]. The microfluidic devices display mainly four structures: the terrace-like device, the T-junction device, the Y-junction device and the flow-focusing device [19].

Microfluidic arrays have been reported for the engineering of lipid nanoparticles for cancer and gene therapy with actually high encapsulation efficiencies in comparison to conventional technologies. For instance, Koh et al. [23] prepared, monodispersed liposomes with smaller size and higher Bcl-2 antisense deoxyoligonucleotide encapsulation efficiencies over bulk methods by using microfluidics [23]. Belliveau et al. [24] used a staggered herringbone micromixer and the prepared LNP siRNA exhibited 50 % target gene silencing in hepatocytes at a dose level of 10 μg/kg siRNA in mice. The produced nanoparticles presented particle sizes of 55 n, with very low polydispersity indexes (0.03) while RNA encapsulation was enhanced (0.25–0.59 mg/ml). Microfluidic arrays have attracted interest for the encapsulation of drug molecules [25], proteins [26]in lipid nanoparticles or the formation of exosomes [26].

Nevertheless, several studies have demonstrated the importance of the microfluidic design, the critical process parameters and material properties (e.g., composition, drug loading). For example, Morikawa et al. investigated different parameters in a microfluidics system such as the Total Flow Rate (TFR) and the Flow Rate Ratio (FRR) that could affect curcumin loaded NPs properties. Interestingly, the encapsulation efficiency of curcumin decreased as the total flow rate increased [27]. Belliveau et al. also investigated the impact of the flow rate on the size and polydispersity of the produced LNPs where passive mixing took place using staggered herringbone patterns. They showed that increasing the total flow rate from 0.02 to 4 ml/min leads to a decrease in the polydispersity of the LNPs. The size of the LNPs stayed constant at flow rates above 2 ml/min [28].

Zhigaltsev et al. explored different flow rate ratios (aqueous/ethanol) and found that a flow rate ratio of 3/1 can generate limit-sized particles [29].

Microfluidic devices were at first fabricated using moulding approaches based on poly(dimethylsiloxane) (PDMS) and thermoplastics e.g., polystyrene, PMMA, polyurethane, etc [30,31]. Moulding is easy to perform and inexpensive but presents some drawbacks such as requiring human labour which makes it hard to use for large scale clinical trials, PDMS is also incompatible with some solvents and their exposure can alter the moulded final device.

3D printing is a technology that can successfully substitute moulding with better outcomes, and as microfluidic devices can be fabricated using a variety additive manufacturing techniques such a stereolithography (SLA), Digital Light Processing (DLP), multi jet modelling (MJM) and Fused Deposition Modelling (FDM) [32,33].

Stereolithography (SLA) is based on the curing of polymer resins where a UV laser hardens the surface via galvanometric mirrors which direct the light and cure the first layer [34]. The build platform moves from the horizontal tank to separate the formed layer and allow fresh resin to flow. The subsequent layers are deposited in the same way until the final shape is obtained and post-curing steps follow the printing process [35]. Similarly, Digital Light Processing (DLP) technology is based on digital micro-mirror device principle, but it projects the light source over the resin. DLP offers faster printing times and similar accuracy compared to SLA [36]. Layers are formed by projecting images of 2D layers from a DLP source and consist of light and dark pixels created by micron-sized mirrors on DMD, which determine the XY-plane resolution of the polymerized layer [37].

This work was twofold where in the first part we have employed DLP printing technology for the fabrication of microfluidic devices of various designs incorporating herringbone structures. Due to the high resolution of the printing resin, it was possible to develop high quality microfluidic devices by varying the number of herringbone structures and the length

of microfluidic channels. In the second part the microfluid designs were assessed for their efficiency to produce liposome nanoparticles by investigating the Total Flow Rate (TFR) and the Flow Rate Ratio (FRR).

2. Materials and methods

2.1. Materials

Lipoid S75 used in this study was obtained from Lipoid GmbH (Ludwigshafen, Germany), Cholesterol and ethanol were obtained from Sigma-Aldrich (UK). Syringe pumps from Harvard Apparatus (Holliston, Massachusetts, USA), were used to control the flow rates of the aqueous and organic phases. Pumps were calibrated accordingly to accurately adjust the Total Flow Rate per minute. Microfluidic resin, MiiCraft BV-007A (Young Optics Inc., Hsinchu, Taiwan) were used to print the microfluidic arrays.

2.2. Design and 3D printing of microfluidic arrays

All three Microfluidic arrays were designed via CAD software (SolidWorks 2018, Dassault Systèmes). All three arrays comprise of two large threaded inlets as show in Fig. 1 designed with 8 mm length at 28 threads per inch. Both threaded inlets are connected to a rectangular channel with a width of 340 μm and a height of 250 μm with its dimensions remaining constant throughout the lengths of the array. Both inlet channels then merge into a single mixing rectangular channel with identical dimensions. As shown in Fig. 1 Array one comprises of 15 cycles where each cycle contains two sequential sections of ridges. Each half cycle has a different orientation. Each ridge has a 50 μm width and 60 μm height while the distance from another is 50 μm. Array 2 consists of 10 cycles and Array 3 of 15 cycles but with shorter total length compared to Array 1.

The microfluidic arrays were printed using a DLP 3D printer (Asiga MAX X27(Asiga, Erfurt, Germany)) equipped with a 385 nm DLP projector with a 27 μm pixel size. The microfluidic arrays were designed via SolidWork Software (SolidWork 2017, Dassault Systems, Waltham, MA, USA). The designs were initially saved as.prt files and then converted into.stl files. The.stl files were then imported into a slicing software Composer (V1.2, Asiga, Germany). The printing orientation was set to 45° inclusive of supports (no internal support) according to our pervious study on the microfluidics resin [38]. The arrays were printed at 25 μm layer thickness with UV intensity set to 3 mW/cm2 and a layer exposure time of 3.3 s. The printed microfluidic arrays were then removed from the build plate followed by gentle removal of the support structures. The array was then soaked in isopropanol for 10 min to eliminate the uncured resin residues on the array's surface. The microfluidic array channels were then coupled to the syringe pump and were flushed using isopropanol repeatedly for 5 cycles to wash out the uncured resins within the channels. The array was then left overnight to dry and then was further cured using a in a UV-A heated chamber (MeccatroniCore BB Cure Dentalstation, GoPrint3D, Ripon, North Yorkshire, UK) with a wavelength of 405 nm for full polymerisation. The curing settings were set at 60 min and at 40 °C which would generate structures with best mechanical performance for the specified resin based on our pervious study [38].

2.3. Liposomes preparation

Empty liposomes were produced using three different 3D printed microfluidics arrays as shown in Fig. 1. The devices were connected to the syringes through tubes and the pumps allowed to adjust Total Flow Rates (TFR) of 3, 5 and 10 ml/min. The organic phase was made of Lipoid S75 and cholesterol both dissolved in ethanol at a ratio of 80:20 **(w/w)** respectively and at a concentration of 50 mg/ml. The aqueous phase was heated at a temperature of 70 °C.

The organic and aqueous phases were introduced in the device through two different inlets, both phases were mixed with herringbone micromixers inside the device. In this study, we used 8:2 and 6:4 Flow Rate Ratios (FRR) between the aqueous and organic phase respectively. The final concentrations of the aqueous phase after EtOH evaporation were 33.33 mg/ml and 12.5 mg/ml for the FRR 6:4 and 8:2 respectively. The liposomes were collected from the single outlet and stirred on a cold plate in order to remove the ethanol. The microfluidic devices were washed with ethanol and water after each triplicate to ensure the channels are not blocked by the lipids before the next formulation.

The Peclet numbers were estimated using the following equation:

$$P_e = \frac{U\,x\,L}{D}, \tag{1}$$

Where U is the average velocity, L the length of the array and D the ethanol-water diffusion coefficient at various molar fractions [39,40].

2.4. Particle size and zeta potential

Liposome size, PDI, mobility and zeta potential were all measured by dynamic light scattering (DLS) performed by (Malvern Zetasizer Nano series, UK). Two drops of our suspension were added to deionised water in the Zetasizer cuvettes to measure the size and zeta potential at 25 °C. Each measurement was carried out in triplicates.

2.5. Statistical analysis

All experiments were performed in triplicates with calculation of means and standard deviations in Excel sheets.

2.6. Stability tests

The stability measurements were taken four weeks after the liposomes preparation, the storage was at 4 °C. Liposome size, PDI, mobility and zeta potential were all measured by dynamic light scattering (DLS) performed by (Malvern Zetasizer Nano series, UK). Each of the measurements was done in triplicates.

2.7. Scanning electron microscopy (SEM)

SEM was used to evaluate the printing accuracy of the DPL technology. For the purpose of the investigation open microfluidic designs were printed featuring the exact same details as the closed arrays. SEM images were captured with Hitachi SU8030, Tokyo, Japan by an electron beam accelerating voltage of 1.0 kV and magnification of 30×.

3. Results and discussion

Microfluidic arrays have shown significant advantages for the engineering of lipid nanoparticles (Zhang et al., 2019). 3D printing is an alternative manufacturing technique for microfluidic arrays that has lately gained popularity, as it has the capability to solve issues related to the poly(dimethylsiloxane) fabricated devices (Chen et al., 2016). A major benefit of 3D printing is the fabrication of robust and complex designs with unique features. In this study the use of DLP offered excellent print resolution and enabled the printing of the designed arrays. The purpose of the study was to assess the mixing efficiency of microfluidic arrays consisting of different designs for the manufacturing of liposome nanoparticles.

As shown in Fig. 1, three microfluidics devices were 3D printed using DLP printer comprising of different designs and series of herringbone structure micromixers to facilitate the mixing of the organic phase and the aqueous phases. The two phases are introduced through different inlets into the device coupled with a dual syringe pump. DLP was selected as the preferred technology due to the excellent capability to fabricate complex geometries with high resolution [41,42]. Practically,

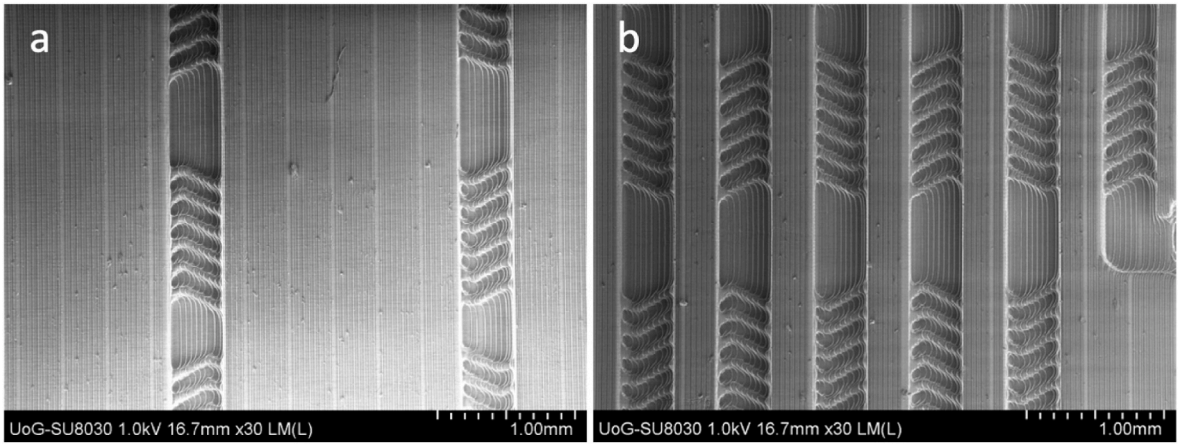

Fig. 2. SEM images of open 3D printed microfluidic Array 2 (a) and Array 3 (b) which shows the high printing accuracy of the staggered herringbone mixers.

Table 1
Summary of Peclet number, particle size, mobility, PDI and ζ-potential measurements of the liposomes based on the TFR and FRR for each microfluidics device.

Flow rate ratio	Total Flow Rate (ml/min)	Device type	*Pe* (x10^7)	Mean size (nm)	Mobility (μmcm/Vs)	PDI	ζ-Potential (mV)
8:2	3	Array1	4.1	70.9 ± 3.3	−4.5 ± 0.2	0.2 ± 0	−58.1 ± 3.6
8:2	3	Array 2	2.7	73.1 ± 2.3	−4.7 ± 0.2	0.2 ± 0	−60.8 ± 3.7
8:2	3	Array 3	3.5	69.3 ± 0.3	−3.9 ± 0.3	0.2 ± 0	−50.0 ± 4.0
8:2	5	Array 1	7.0	53.8 ± 1.1	−3.6 ± 0.4	0.2 ± 0	−46.1 ± 6.3
8:2	5	Array 2	4.4	52.6 ± 0.6	−4.7 ± 0.3	0.2 ± 0	−60.6 ± 4.5
8:2	5	Array 3	5.8	60.1 ± 1.1	−4.6 ± 0.2	0.3 ± 0	−58.7 ± 3.0
8:2	10	Array 1	14.0	41.5 ± 1.5	−2.7 ± 0.1	0.2 ± 0	−44.8 ± 2.3
8:2	10	Array 2	9.0	40.5 ± 0.2	−2.9 ± 0.2	0.2 ± 0	−48.0 ± 3.4
8:2	10	Array 3	11.6	44.1 ± 3.6	−4.8 ± 0.3	0.3 ± 0	−62.0 ± 4.1

it was possible to adjust the geometry of the herringbone structures and features such as height, width, and length while printing arrays of high quality. The robustness of the arrays was further improved by using layer heights varying from 25 to 50 μm. The technology is labour saving due to the low cost of the resin while multiple arrays can be printed simultaneously within few hours. This is a significant accomplishment that allows customization of the array designs to meet different specifications of a given nanoparticulate system in comparison to the costly commercial microfluidic devices. As shown in Fig. 1S (supplementary material) the use of a transparent resin allows the optical observation of aqueous and organic flows (use of a blue and red dye) that demonstrates the excellent mixing performance of the printed arrays.

Fig. 2 shows SEM micrographs of the microfluidic arrays where distinct herringbone structures with repeated units can be observed. It can be seen that in each mixing channel, four units comprising of 5 herringbone structures each were placed to facilitate chaotic advection of the laminar streams resulting fast mixing of the organic and aqueous phases. No defects of the herringbone structures could be observed suggesting DLP printing is an ideal technology for the manufacturing of microfluidic arrays.

For the purposes of the study Lipoid S75 was selected as the main

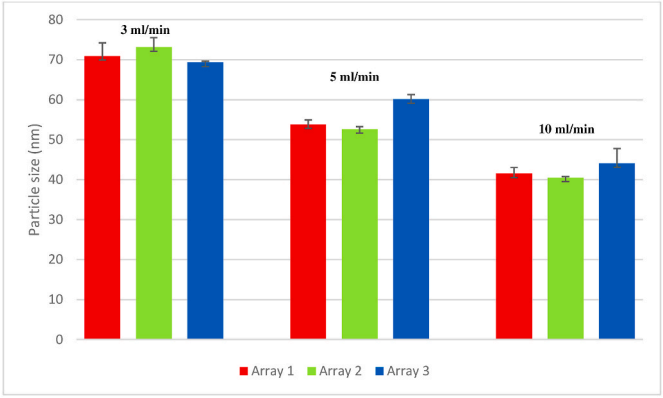

Fig. 3. Mean particle size of the liposomes using three different array designs at Total Flow Rates of 3, 5 and 10 ml/min and at a Flow Rate Ratio of 8:2.

Table 2
Summary of Peclet number, particle size, mobility, PDI and ζ-potential measurements of the liposomes based on the TFR and FRR for each microfluidics device.

Flow rate ratio	Total Flow Rate (ml/min)	Device type	*Pe* (x10^7)	Mean size (nm)	Mobility (μmcm/Vs)	PDI	ζ-Potential (mV)
6:4	3	Array 1	9.4	86.6 ± 0.2	−5.1 ± 0.3	0.2 ± 0	−65.9 ± 4.8
6:4	3	Array 2	6.0	76.1 ± 0.8	−3.5 ± 0.2	0.2 ± 0	−44.7 ± 3.0
6:4	3	Array 3	7.9	75.8 ± 2.5	−3.6 ± 0.4	0.2 ± 0	−46.6 ± 6.1
6:4	5	Array 1	15.7	72.5 ± 2.4	−4.1 ± 0.5	0.2 ± 0	−53.2 ± 7.0
6:4	5	Array 2	10.1	71.6 ± 3.0	−4.1 ± 0.4	0.2 ± 0	−52.4 ± 5.8
6:4	5	Array 3	13.2	78.2 ± 5.6	−5.0 ± 0.3	0.2 ± 0	−64.5 ± 4.4
6:4	10	Array 1	31.4	55.1 ± 1.9	−4.5 ± 0.3	0.3 ± 0	−58.6 ± 4.5
6:4	10	Array 2	20.1	51.9 ± 4.4	−4.4 ± 0.5	0.4 ± 0.1	−56.2 ± 6.5
6:4	10	Array 3	26.4	48.8 ± 2.4	−3.8 ± 0.4	0.3 ± 0	−49.7 ± 5.4

Table 3
Summary of Peclet number, particle size, mobility, PDI and ζ-potential measurements of the liposomes based on the TFR and FRR for each microfluidics device and for a final lipid concentration of 12.5 mg/ml.

Flow rate ratio	Total Flow Rate (ml/min)	Device type	*Pe* (x10^7)	Mean size (nm)	Mobility (μmcm/Vs)	PDI	ζ-Potential (mV)
6:4	10	Array1	31.4	49.3 ± 2.5	−3.1 ± 0.4	0.2 ± 0	−39.8 ± 5.5
6:4	10	Array 2	20.1	45.2 ± 2.7	−3.4 ± 0.2	0.2 ± 0	−44 ± 3.0

lipid and cholesterol for enhanced nanoparticle stability at a fixed ratio of 80:20 (w/w). The targeted liposome concentration was 10 mg/mL but preliminary data (flat microfluidic arrays) showed that concentrations up to 30 mg/mL can be attained. The preferred Flow Rate Ratios (FRR) of the aqueous and organic phases were set at 8:2 and 6:4 while three different Total Flow Rates (TFR) at 3, 5 and 10 mL/min were assessed for each array. In previous studies Lamprou et al. (2016) and Hamano et al. (2019) used FRR (of 1:1, 3:1 and 5:1 [[43,44]] but according to our preliminary work increase amounts of organic phase reduced the nanoparticle stability. Furthermore, an 8:2 w/w lipid to cholesterol (CH) ratio was used in order to enhance liposome rigidity and stability. The CH ratio can vary from 10 to 50 % w/w depending on the liposome formulation. It is known that the zeta potential of formed nanoparticles provides insights about the liposome stability. As shown in Tables 1 and 2, zeta values varied from −40 to −60 mV indicating excellent stability for all nano dispersions.

In Fig. 3, all array designs showed the formation of less than 100 nm of liposome nanoparticles even at TFRs of 3 ml/min, which is quite below the reported values obtained by other research groups (Lamprou et al., 2016 and Hamano et al., 2019)). It is believed that this is due to the specific design of the herringbone micromixers. From Fig. 3 it is also evident that for each array, the particle size decreases with increasing TFR from 3 to 10 ml/min. By increasing the TFR the mixing time and hence diffusion between the organic and aqueous phases is shorter. At higher TFR, the increased mixing of the two phases induces chaotic advection of the laminar flows resulting in smaller particle sizes of the formed nanoparticles. As shown in Fig. 3, a significant particle size reduction from 71 to 42 nm was observed. However, other studies showed that the TFR has no impact on the particle size reduction in contrast to our findings [[41,45]]. Nevertheless, our findings regarding the TFR impact on the particle size reduction are in good agreement with Feng et al. (2015) who demonstrated that higher flow rates led to the formation of smaller particles with narrower size distribution [46]. As shown in Fig. 1 the arrays comprise of different channel lengths numbers of herringbone structures. Interestingly, the design of the arrays had no effect on the particle size reduction and similar results were obtained under the same TFR and FRR.

The fact that the three different designs didn't affect the particle size significantly is related to the total number of cycles of each array. Maeki et al. (2015), prepared LNPs using SHM with different cycles. It was shown that for SHM with more than 10 cycles the obtain particle sizes were not further reduced. Further particle size reduction was only achieved by increasing the FRR as in our case (8:2 vs. 6:4). The printed Arrays 1–3 comprise of 15, 10 and 15 cycles respectively and this is why the formed liposomes presented similar particle size. This is more evident for Arrays 1 and 3 which have 15 cycles but with different lengths. Even though different array length (L) resulted in different *Pe* numbers (Eq. (1)) the particle size was only influence by the TFR and FRR.

Further investigation included the comparison of liposome formulations under the same lipid/cholesterol concentration but at different FRRs. We also compared formulations with the same final lipid concentration but different FRRs. As shown in Table 3 liposomes with 12.5 mg/ml total lipid concentration were prepared using FRR of 6:4 and compared to those made at 8:2 (Table 1).

The obtained particle size confirmed the assumption that FFRs with higher molar fractions of organic phase (6:4) produce larger LPNs compared those with reduced EtOH amounts (8:2). In addition, it is

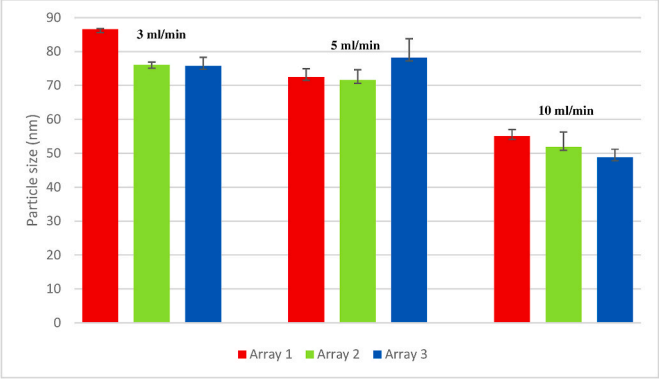

Fig. 4. Mean particle size of the liposomes using three different array designs at Total Flow Rates of 3, 5 and 10 ml/min and at a Flow Rate Ratio of 6:4.

obvious that lower lipid concentrations produced small nanoparticles when using the same FFR. Hence, for FFR 6:4 and 33.3 mg/ml total lipid concentration, Arrays 1 and 2 produced liposomes o 51.9 nm and 48.8 nm while for 12.5 mg/ml the obtained particles were 49.3 nm and 45.2 nm respectively.

By observing Fig. 4, the increase of the organic phase ratio from 8:2 to 6:4 showed a slightly negative effect in the obtained particle size of nanoparticles for all arrays. For TFR varying from 3 to 10 ml/min, a 10–20 nm particle size increase was observed. Hence the increase of the fraction of the organic phase resulted in the formation of larger liposomes. Interestingly the PDI, zeta potential and mobility were not altered by the change of the FRR from 8:2 to 6:4. Similarly to the previous TFR findings the microarray designs did not reveal any significant difference in the particle size for the obtain nanoparticles.

The z-potential of the produced liposomes for the three microfluidic arrays varied from −45 mV to 64 mV. The values of z-potential are relatively constant for all Arrays with small variation which however, did not reveal any significant trends. This range is a strong indication for good electrostatic stabilization due to the mutual repulsion of liposomes [47].

Overall, the experimental findings are in good agreement with previous studies (Kaster et al.) as the three microfluidic arrays produced nanoparticles varying from 40 to 90 nm. A careful look in previous studies (Karster, Lamprou) reveals that beyond the TFR and FFR other factors have a significant impact on the obtained liposome particle size. Those are:

a) The dimensions of the microfluidic channels: It is known that flow supports such as micromixing structures promote mixing efficiency and smaller particle sizes. Thus, the presence of herringbone structures in our printed arrays significantly reduced the particle size. The absence of micromixing structures produced nanoparticles of 120–180 nm (data not shown). This claim was also supported by Marschewski et al. who demonstrated that flow promoters exhibit turbulent flow at high flow rates and hence better mixing capacity [48]. Furthermore, the channel cross-section affects the extent of mixing where for small channels mixing time are shorter but the optimal TFR should be identified (Belliveau et al., 2012).
b) The lipid content: in general increase of the lipid concentration is accompanied by decrease of the nanoparticle size as shown by

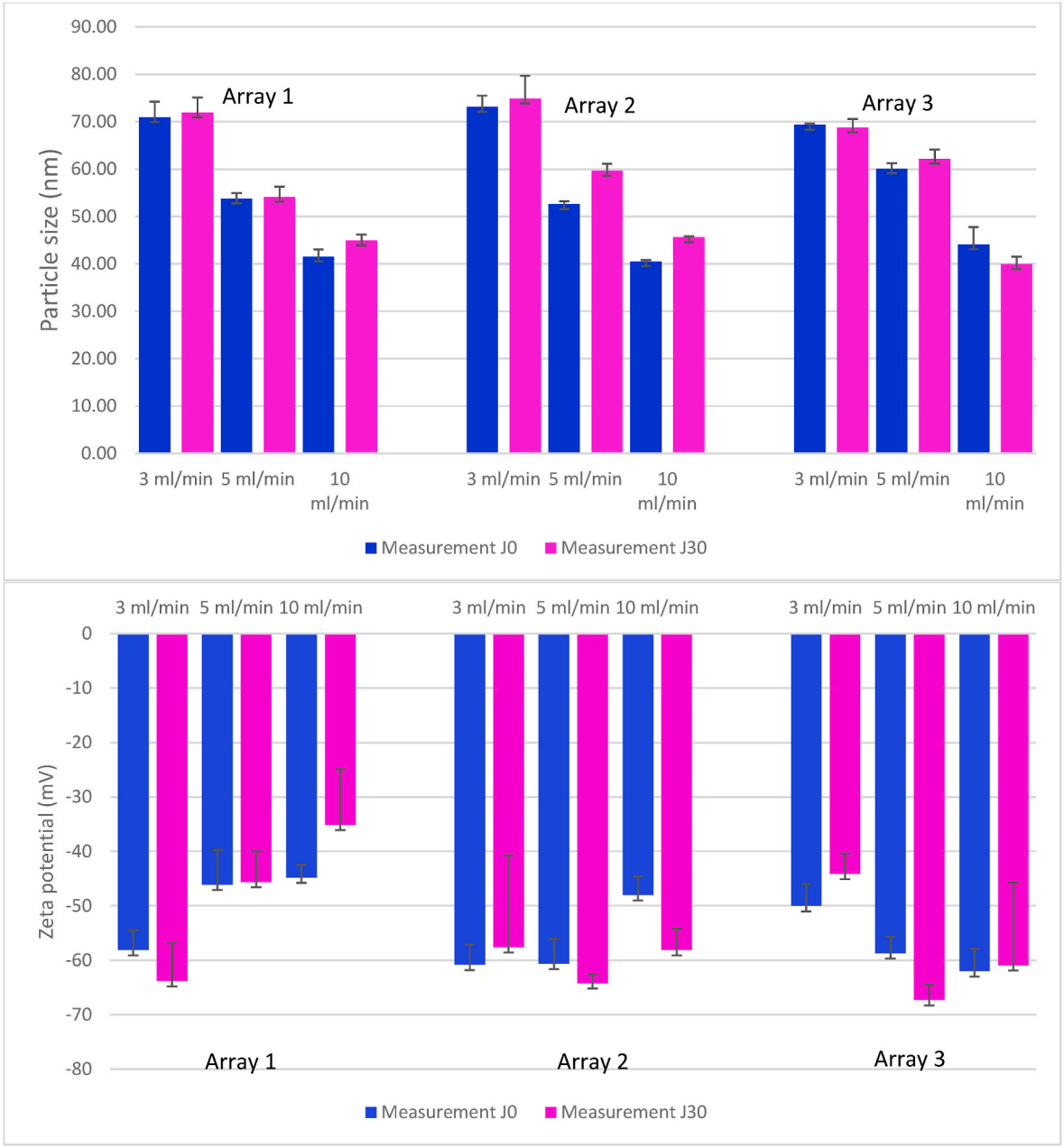

Fig. 5. Mean particle size and ζ-potential of liposomes prepared via different array designs at Total Flow Rates of 3, 5 and 10 ml/min and at a Flow Rate Ratio of 8:2 after 4 weeks storage.

Karster et al. Nevertheless, the use of polar lipids has shown a particle size increase when using higher proportions (Belliveau et al., 2012).

c) The cholesterol, which plays an important role on the rigidity and stability of liposome nanoparticles has been found to increase the average particle size with increased CH content (Lee et al., 2005).

The study demonstrates the successful use of 3D printed microfluidic arrays for the design and development of liposome nanoparticles. Microfluidic devices with staggered herringbone micromixers are commercially available (NanoAssemblr, Precision NanoSystems, Canada). Which offer user-friendly automated operating system that are used for the engineering of LNPs. By using DLP, we were able to print microfluidic devices with unique geometries, similar to the marketed arrays, in a rapid (roughly 2 h for up to three arrays) and cost-effective manner. The arrays can be printed without any defects by varying the channel cross-section, channel length and herringbone dimensions for achieving rigorous and chaotic mixing of the two flows.

On the other hand, FDM devices were reported to have a limited ability to create smaller channels while they display a higher surface roughness [49] SLA/DLP devices were found to show a better resolution and a smooth surface over FDM ones. Macdonald et al. compared FDM and DLP devices and reported that the surface roughness of FDM devices was around 31 times greater than the surface roughness of DLP devices [50]. Furthermore, FDM devices are typically not completely transparent once printed unlike the DLP ones.

3.1. Stability studies

The stability of the particle size and zeta potential of the liposomes prepared by the different microfluidic arrays were further determined after one month. As it can be seen in Figs. 5–6 only negligible changes

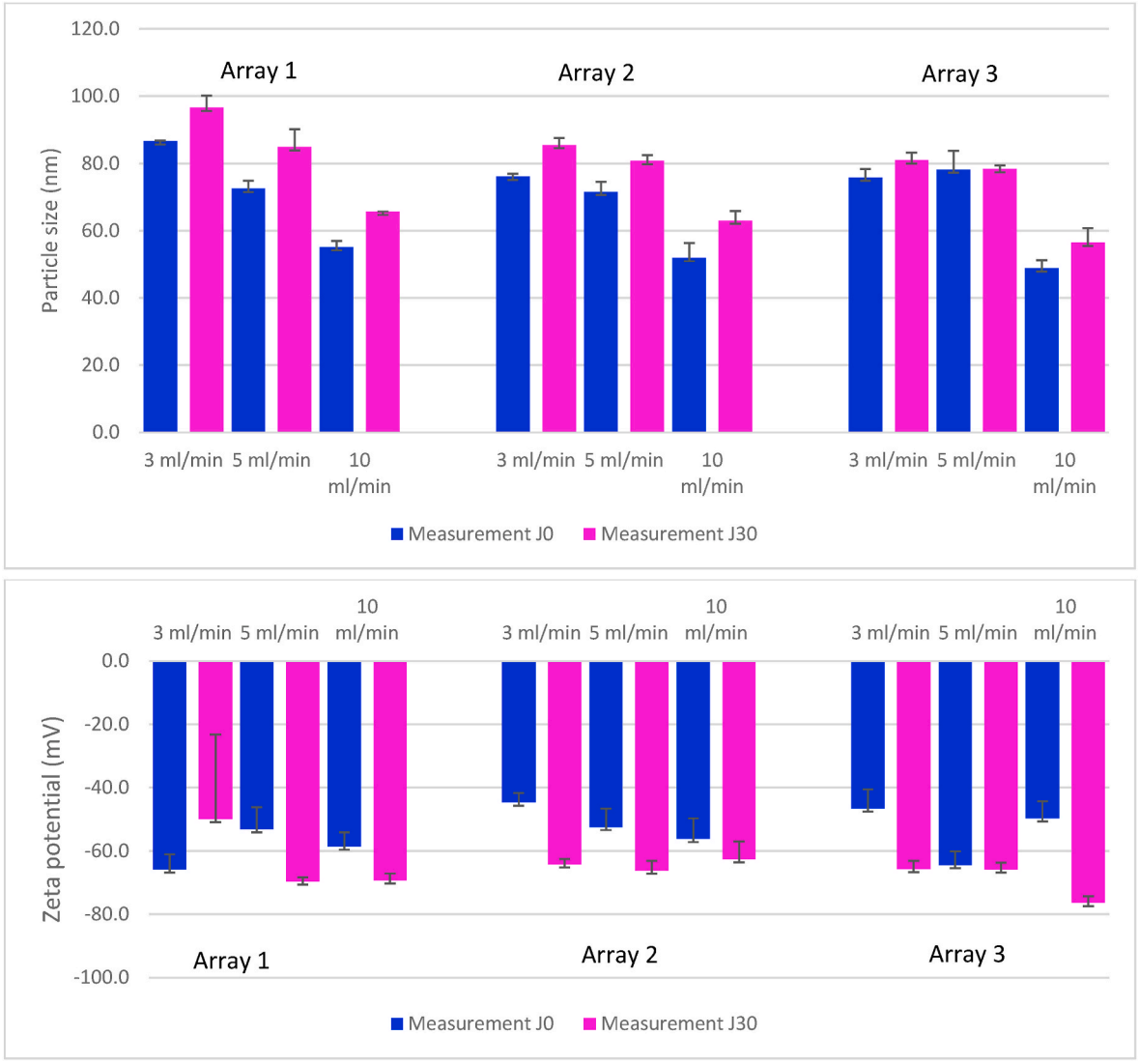

Fig. 6. Mean particle size and ζ-potential of the liposomes prepared via different array designs at Total Flow Rates of 3, 5 and 10 ml/min and at a Flow Rate Ratio of 6:4 after 4 weeks storage.

could be observed for both the particle size and zeta potential. The microfluidic made nanoparticles were very stable irrespectively of the microfluidic array used for the preparation at 8:2 FRRs. A small particle size increase of 8–10 nm was observed for some nano-dispersions for FRR of 6:4 accompanied with changes in the ζ-potential varying form 5–8 mV. The stability of the liposomes was mainly attributed to the lipid composition which resulted in high z-potential values but also on the effect of the microfluidic arrays which resulted in monodispersed particle size distributions with low PDIs.

4. Conclusion

DLP technology was employed for the printing of microfluidic arrays and the production of liposome nanoparticles. The arrays featured herringbone structures of varying numbers and microfluidic channel lengths. The formation of liposomes was found to depend on the TFR and FRR and the obtained particle sizes varied from 40 to 90 nm. The design of the microfluidic arrays did not impact the size of the formed liposomes. By employing DLP it was feasible to fabricate cost effective and highly accurate microfluidic arrays with complex structures for the engineering of liposome nanoparticles.

CRediT authorship contribution statement

Kanza Rahali: Data curation, Formal analysis, Investigation, Methodology, Validation, Writing – original draft. **Atabak Ghanizadeh Tabriz:** Data curation, Formal analysis, Investigation, Methodology, Software, Validation, Writing – original draft. **Dennis Douroumis:** Conceptualization, Data curation, Funding acquisition, Methodology, Project administration, Resources, Writing – original draft, Writing – review & editing.

Declaration of competing interest

The authors declare that they have no known competing financial interests or personal relationships that could have appeared to influence the work reported in this paper.

Data availability

Data will be made available on request.

Appendix A. Supplementary data

Supplementary data to this article can be found online at https://doi.org/10.1016/j.jddst.2024.105411.

References

[1] W. Li, N. Little, J. Park, C.A. Foster, J. Chen, J. Lu, Tumor-associated fibroblast-targeting nanoparticles for enhancing solid tumor therapy: progress and challenges, Mol. Pharm. 18 (2021) 2889–2905.
[2] D. Chatzikleanthous, D.T. O'Hagan, R. Adamo, Lipid-based nanoparticles for delivery of vaccine adjuvants and antigens: toward multicomponent vaccines, Mol. Pharm. 18 (2021) 2867–2888.
[3] P. Kazemian, S.-Y. Yu, S.B. Thomson, A. Birkenshaw, B.R. Leavitt, C.J.D. Ross, Lipid-nanoparticle-based delivery of CRISPR/Cas9 genome-editing components, Mol. Pharm. 19 (2022) 1669–1686.
[4] M. Klein-Hitpaß, J.-E. Ostwaldt, C. Schmuck, M. Giese, Water-soluble, pH responsive polymeric nanoparticles: a modular approach, ACS Appl. Polym. Mater. 2 (2020) 2499–2503.
[5] M. Rui, Y. Xin, R. Li, Y. Ge, C. Feng, X. Xu, Targeted biomimetic nanoparticles for synergistic combination chemotherapy of paclitaxel and doxorubicin, Mol. Pharm. 14 (2017) 107–123.
[6] D. Chatzikleanthous, D.T. O'Hagan, R. Adamo, Lipid-based nanoparticles for delivery of vaccine adjuvants and antigens: toward multicomponent vaccines, Mol. Pharm. 18 (2021) 2867–2888.
[7] Z.R. Sia, M.S. Miller, J.F. Lovell, Engineered nanoparticle applications for recombinant influenza vaccines, Mol. Pharm. 18 (2021) 576–592.
[8] P. Ning, H. Yao, F. Du, et al., Gene reprogramming armed macrophage membrane-camouflaged nanoplatform enhances bionic targeted drug delivery to solid tumor for synergistic therapy, Mol. Pharm. 20 (2023) 2362–2375.
[9] M. Rui, Y. Xin, R. Li, Y. Ge, C. Feng, X. Xu, Targeted biomimetic nanoparticles for synergistic combination chemotherapy of paclitaxel and doxorubicin, Mol. Pharm. 14 (2017) 107–123.
[10] K.G. Gareev, D.S. Grouzdev, V.V. Koziaeva, et al., Biomimetic nanomaterials: diversity, technology, and biomedical applications, Nanomaterials 12 (2022) 2485.
[11] C.Y. Beh, R.P. Prajnamitra, L.-L. Chen, P.C.-H. Hsieh, Advances in biomimetic nanoparticles for targeted cancer therapy and diagnosis, Molecules 26 (2021) 5052.
[12] M. Niu, Y.W. Naguib, A.M. Aldayel, et al., Biodistribution and *in vivo* activities of tumor-associated macrophage-targeting nanoparticles incorporated with doxorubicin, Mol. Pharm. 11 (2014) 4425–4436.
[13] A.R. Bhide, M. Suri, S. Katnoria, et al., Evaluation of pharmacokinetics, biodistribution, and antimalarial efficacy of artemether-loaded polymeric nanorods, Mol. Pharm. 20 (2023) 118–127.
[14] J.A. Mills, J. Humphries, J.D. Simpson, S.E. Sonderegger, K.J. Thurecht, N. L. Fletcher, Modulating macrophage clearance of nanoparticles: comparison of small-molecule and biologic drugs as pharmacokinetic modifiers of soft nanomaterials, Mol. Pharm. 19 (2022) 4080–4097.
[15] A. Albanese, P.S. Tang, W.C.W. Chan, The effect of nanoparticle size, shape, and surface chemistry on biological systems, Annu. Rev. Biomed. Eng. 14 (2012) 1–16.
[16] Y. Liu, G. Yang, Y. Hui, S. Ranaweera, C. Zhao, Microfluidic nanoparticles for drug delivery, Small 18 (2022) 2106580.
[17] P.M. Valencia, O.C. Farokhzad, R. Karnik, R. Langer, Microfluidic technologies for accelerating the clinical translation of nanoparticles, Nat. Nanotechnol. 7 (2012) 623–629.
[18] R. Ran, A.P.J. Middelberg, C.-X. Zhao, Microfluidic synthesis of multifunctional liposomes for tumour targeting, Colloids Surf. B Biointerfaces 148 (2016) 402–410.
[19] E. Chiesa, R. Dorati, S. Pisani, et al., The microfluidic technique and the manufacturing of polysaccharide nanoparticles, Pharmaceutics 10 (2018) 267.
[20] T.J. Kwak, Y.G. Nam, M.A. Najera, S.W. Lee, J.R. Strickler, W.-J. Chang, Convex grooves in staggered herringbone mixer improve mixing efficiency of laminar flow in microchannel, PLoS One 11 (2016) e0166068.
[21] H.H. Bau, J. Zhong, M. Yi, A minute magneto hydro dynamic (MHD) mixer, Sens. Actuators, B 79 (2001) 207–215.
[22] A.D. Stroock, S.K.W. Dertinger, A. Ajdari, I. Mezić, H.A. Stone, G.M. Whitesides, Chaotic mixer for microchannels, Science 295 (2002) 647–651, 1979.
[23] C.G. Koh, X. Zhang, S. Liu, et al., Delivery of antisense oligodeoxyribonucleotide lipopolyplex nanoparticles assembled by microfluidic hydrodynamic focusing, J. Contr. Release 141 (2010) 62–69.
[24] N.M. Belliveau, J. Huft, P.J. Lin, et al., Microfluidic synthesis of highly potent limit-size lipid nanoparticles for in vivo delivery of siRNA, Mol. Ther. Nucleic Acids 1 (2012) e37.
[25] D. Mendanha, S. Gimondi, B.M. Costa, H. Ferreira, N.M. Neves, Microfluidic-derived docosahexaenoic acid liposomes for glioblastoma therapy, Nanomedicine 53 (2023) 102704.
[26] M. Tsakiri, A. Ghanizadeh Tabriz, N. Naziris, K. Rahali, D. Douroumis, C. Demetzos, Exosome-like genistein-loaded nanoparticles developed by thin-film hydration and 3D-printed Tesla microfluidic chip: a comparative study, Int. J. Pharm. (2024) 123788.
[27] Y. Morikawa, T. Tagami, A. Hoshikawa, T. Ozeki, The use of an efficient microfluidic mixing system for generating stabilized polymeric nanoparticles for controlled drug release, Biol. Pharm. Bull. 41 (2018) 899–907.
[28] N.M. Belliveau, J. Huft, P.J. Lin, et al., Microfluidic synthesis of highly potent limit-size lipid nanoparticles for in vivo delivery of siRNA, Mol. Ther. Nucleic Acids 1 (2012) e37.
[29] I.V. Zhigaltsev, N. Belliveau, I. Hafez, et al., Bottom-up design and synthesis of limit size lipid nanoparticle systems with aqueous and triglyceride cores using millisecond microfluidic mixing, Langmuir 28 (2012) 3633–3640.
[30] H. Becker, Polymer microfluidic devices, Talanta 56 (2002) 267–287.
[31] E.K. Sackmann, A.L. Fulton, D.J. Beebe, The present and future role of microfluidics in biomedical research, Nature 507 (2014) 181–189.
[32] N. Bhattacharjee, A. Urrios, S. Kang, A. Folch, The upcoming 3D-printing revolution in microfluidics, Lab Chip 16 (2016) 1720–1742.
[33] S. Khorshid, M. Montanari, S. Benedetti, et al., A microfluidic approach to fabricate sucrose decorated liposomes with increased uptake in breast cancer cells, Eur. J. Pharm. Biopharm. 178 (2022) 53–64.
[34] H. Li, W. Fan, X. Zhu, Three-dimensional printing: the potential technology widely used in medical fields, J. Biomed. Mater. Res. 108 (2020) 2217–2229.
[35] R.J. Mondschein, A. Kanitkar, C.B. Williams, S.S. Verbridge, T.E. Long, Polymer structure-property requirements for stereolithographic 3D printing of soft tissue engineering scaffolds, Biomaterials 140 (2017) 170–188.
[36] D.W. Monk, R.O. Gale, The digital micromirror device for projection display, Microelectron. Eng. 27 (1995) 489–493.
[37] R. Chaudhary, P. Fabbri, E. Leoni, F. Mazzanti, R. Akbari, C. Antonini, Additive manufacturing by digital light processing: a review, in: Progress in Additive Manufacturing, 2022.
[38] A.G. Tabriz, B. Viegas, M. Okereke, et al., Evaluation of 3D printability and biocompatibility of microfluidic resin for fabrication of solid microneedles, Micromachines 13 (2022) 1368.
[39] J. Winkelmann, Diffusion coefficient of ethanol in octan-1-ol, in: Diffusion in Gases, Liquids and Electrolytes, Springer Berlin Heidelberg, Berlin, Heidelberg, 2018, p. 313, 313.
[40] The mutual diffusion coefficient of ethanol–water mixtures: determination by a rapid, new method, Proc. Royal Soc. London Math. Phys. Sci. 336 (1974) 393–406.
[41] S.N. Economidou, D.A. Lamprou, D. Douroumis, 3D printing applications for transdermal drug delivery, Int. J. Pharm. 544 (2018) 415–424.
[42] S.N. Economidou, D. Douroumis, 3D printing as a transformative tool for microneedle systems: recent advances, manufacturing considerations and market potential, Adv. Drug Deliv. Rev. 173 (2021) 60–69.
[43] M. Guimarães Sá Correia, M.L. Briuglia, F. Niosi, D.A. Lamprou, Microfluidic manufacturing of phospholipid nanoparticles: stability, encapsulation efficacy, and drug release, Int. J. Pharm. 516 (2017) 91–99.
[44] N. Hamano, R. Böttger, S.E. Lee, et al., Robust microfluidic technology and new lipid composition for fabrication of curcumin-loaded liposomes: effect on the anticancer activity and safety of cisplatin, Mol. Pharm. 16 (2019) 3957–3967.
[45] A. Jahn, S.M. Stavis, J.S. Hong, W.N. Vreeland, D.L. DeVoe, M. Gaitan, Microfluidic mixing and the formation of nanoscale lipid vesicles, ACS Nano 4 (2010) 2077–2087.
[46] Q. Feng, L. Zhang, C. Liu, et al., Microfluidic based high throughput synthesis of lipid-polymer hybrid nanoparticles with tunable diameters, Biomicrofluidics 9 (2015) 052604.
[47] G. Perli, A.C.S.N. Pessoa, T.A. Balbino, L.G. de la Torre, Ionic strength for tailoring the synthesis of monomodal stealth cationic liposomes in microfluidic devices, Colloids Surf. B Biointerfaces 179 (2019) 233–241.
[48] J. Marschewski, S. Jung, P. Ruch, et al., Mixing with herringbone-inspired microstructures: overcoming the diffusion limit in co-laminar microfluidic devices, Lab Chip 15 (2015) 1923–1933.
[49] J. Collingwood, K. De Silva, K. Arif, High-speed 3D printing for microfluidics: opportunities and challenges, Mater. Today: Proc. (2023). https://doi.org/10.1016/j.matpr.2023.05.683.
[50] N.P. Macdonald, J.M. Cabot, P. Smejkal, R.M. Guijt, B. Paull, M.C. Breadmore, Comparing microfluidic performance of three-dimensional (3D) printing platforms, Anal. Chem. 89 (2017) 3858–3866.